Challenges and opportunities in quantitative brain PET imaging

Lopes Alves, Isadora

2

Dual time point method for the quantification of irreversible tracer kinetics:

a reference tissue approach applied to [^{18}F]-FDOPA brain PET

Author(s): *Isadora Lopes Alves*, Sanne K. Meles, Antoon T.M. Willemsen, Rudi A.J.O. Dierckx, Ana M. Marques da Silva, Klaus L. Leenders, Michel Koole

*as published in the Journal of Cerebral Blood Flow and Metabolism (*Alves IL et al, 2016*)*

Introduction

Positron Emission Tomography (PET) provides quantitative information on physiological processes and functional tissue characteristics. The underlying mechanisms of PET tracer binding can be described by compartmental models. However, a model accounting for all states of tracer binding is often too complex and unpractical in a clinical setting. Therefore, model simplifications are essential to provide stable and reliable quantitative endpoints while reducing the acquisition time and/or avoiding invasive procedures such as arterial blood sampling. Especially for PET tracers which bind irreversibly and often require relatively long acquisition times, reducing the scan duration can be imperative to improve patient comfort and clinical applicability.

The Patlak Graphical Analysis[1] (PGA) is a non-compartmental approach to quantify irreversible tracer binding by estimating the metabolization, influx or trapping rate constant of the tracer (K_i). PGA uses the tracer concentration in arterial plasma as input function, and assumes that at some time point post injection an equilibrium is reached between the non-specific, reversible tracer binding in the target tissue and the plasma activity levels. From that time point, the Patlak plot becomes linear and the slope of the linear part corresponds to K_i. If a tissue devoid of specific tracer binding or metabolism is available, it can be considered as a reference tissue. The tracer uptake in this reference tissue can therefore be used as an input function for PGA_{REF}, avoiding the need for arterial blood sampling[2]. Despite the fact that quantifying irreversible tracer binding using PGA or PGA_{REF} is rather straightforward, irreversible tracer kinetics are often quantified by one static scan at a late time point post injection (p.i.). This approximation reduces the scanning time, therefore increasing cost effectiveness and patient comfort while minimizing motion artifacts. Tracer uptake values of this static scan can be converted to Standardized Uptake Values (SUV)[3] by normalizing for injected dose and patient weight. They can also be normalized to the tracer uptake in a reference tissue or to blood activity levels, yielding SUV ratio values (SUVR)[4,5]. However, quantification using one static scan at a fixed, late time point p.i. has several drawbacks, extensively described for oncological [^{18}F]-FDG[6,7] PET imaging. Amongst the most important limitations are the

dependency of the quantification on the imaging time point p.i.[3] and the lack of direct information on the trapping or metabolization rate[8] of the tracer.

To overcome the limitations of a SUV based quantification, a dual time point (DTP) method was proposed for [^{18}F]-FDG PET imaging[9] as an approximation for PGA. The DTP method estimates K_i using the tissue tracer concentration and blood activity levels of two late static scans. Therefore, it potentially reduces acquisition times and increases patient comfort while providing equivalent quantitative information. We extended the previous DTP method to a reference tissue approach (DTP_{REF}) such that PET imaging of irreversibly tracer binding could also benefit from a DTP quantification when a reference tissue is available.

[^{18}F]-FDOPA[10] is a PET tracer with irreversible binding characteristics and well-established for the diagnosis and progression assessment of Parkinson's Disease (PD)[11], a disorder characterized by the loss of presynaptic dopaminergic neurons. After entering the brain, [^{18}F]-FDOPA is decarboxylated into [^{18}F]-dopamine and trapped in the presynaptic vesicles. Nonetheless, a small fraction of [^{18}F]-dopamine is metabolized and excreted from the brain. In addition, an [^{18}F]-FDOPA metabolite formed in plasma is able to cross the blood-brain barrier and enter the brain. Due to its complex metabolic pathway and the presence of metabolites, [^{18}F]-FDOPA has been quantified by several models[12–16], each of them focusing on specific parts of the tracer kinetic profile. However, for the first 90 min after injection, [^{18}F]-FDOPA is considered to bind irreversibly[17], with PGA being widely applied for its quantification. Moreover, the occipital cortex can be used as a reference tissue representing the reversible and non-displaceable uptake of [^{18}F]-FDOPA in brain tissue and enabling the use of both PGA_{OCC} and SUVR approaches[12]. More specifically, the striatal uptake of [^{18}F]-FDOPA relative to the occipital cortex is denoted striatal-to-occipital ratio (SOR).

The present study had two goals. The first goal was to derive a DTP_{REF} method based on a reference tissue approach and validate this method for the quantification of [^{18}F]-FDOPA brain scans using the occipital cortex as reference region (DTP_{OCC}). The second goal was to evaluate the performance of the DTP_{OCC} model in differentiating patients with Parkinson's disease from healthy controls. For this purpose, the DTP_{OCC} approach was compared to the

standard PGA_{OCC} model using a full dynamic PET scan and to the clinically relevant SOR using a late static PET scan.

Material and Methods

Theory

Similar to the approach of van den Hoff and colleagues[9], we derived the DTP_{REF} method directly from the PGA_{REF} equations. PGA_{REF} describes the tissue tracer concentration at a specific time point t post-injection (p.i.) using a reference tissue model as follows[2]:

$$\frac{C_T(t)}{C_R(t)} = K_i^{REF} \frac{\int_0^t C_R(\tau)d\tau}{C_R(t)} + V_R \quad (1)$$

with $C_T(t)$ and $C_R(t)$ the tracer concentration in target and reference region, respectively. K_i^{REF} represents the influx rate K_i relative to the non-displaceable and reversible tracer binding under the assumption that the ratio of rate constants describing tracer exchange between plasma and brain tissue is identical for target and reference tissue. V_R is the apparent distribution volume of the non-displaceable and reversible tracer binding in the target tissue relative to the reference tissue. Hence, PGA_{REF} plots the ratio between target and reference tissue uptake (SUVR) as function of a "Reference Patlak time" (RPT), which corresponds to the area under the time activity curve of the reference tissue, normalized to its instantaneous tracer concentration.

If we can assume that from a time point t^* p.i. the tracer concentration in the reversible and non-displaceable compartment of the target tissue and the tracer concentration in the reference tissue both follow the plasma concentration, their ratio becomes constant. Once this equilibrium is reached, the PGA_{REF} plot becomes linear and its slope represents K_i^{REF}. As a result, the tracer uptake at two time points $t_1 > t$ and $t_2 > t_1$ p.i. can be described as:

$$SUVR(t_1) = K_i^{REF} RPT(t_1) + V_R \quad (2)$$

$$SUVR(t_2) = K_i^{REF} RPT(t_2) + V_R \quad (3)$$

Subtracting Equation (2) from Equation (3) and isolating K_i^{REF} yields:

$$K_i^{REF} = \frac{SUVR(t_2) - SUVR(t_1)}{RPT(t_2) - RPT(t_1)} \quad (4)$$

The nominator terms of Equation (4) can be estimated directly from two static scans acquired at time points t_1 and t_2. The first integral term in the denominator can be expanded as:

$$RPT(t_2) = \frac{\int_0^{t_1} C_R(t)dt + \int_{t_1}^{t_2} C_R(t)dt}{C_R(t_2)} = \frac{C_R(t_1) RPT_{REF}(t_1)}{C_R(t_2)} + \frac{\int_{t_1}^{t_2} C_R(t)dt}{C_R(t_2)} \quad (5)$$

The second term of equation (5) can be estimated from the same two static scans by a trapezoid approximation. However, the first term involves $RPT(t_1)$, which is also explicitly present in Equation (4) and which requires information on the tracer uptake from the start of the scan until the first time point t_1. Under the assumption that for this time interval inter-patient variability of the normalized area under the curve of the reference tissue is sufficiently small, a population based average can be used as an approximation for the individual $RPT(t_1)$.

Consequently, once the population $\overline{RPT}(t_1)$ is determined and Equation (5) is computed, the influx rate constant can be determined using a DTP_{REF} method as:

$$K_{DTP}^{REF} = \frac{SUVR(t_2) - SUVR(t_1)}{RPT(t_2) - \overline{RPT}(t_1)} \quad (6)$$

The application of this method requires only 1) the tracer concentration in the target and the reference tissue from two static scans at different time points t_1 and t_2 p.i. and 2) a population based average $\overline{RPT}(t_1)$ for the first time point t_1.

[^{18}F]-FDOPA dynamic PET study

Data from 18 subjects included in a clinical study performed at the University Medical Center Groningen (UMCG) were retrospectively analyzed. Written informed consent was obtained according to the 1964 Helsinki declaration and its later amendments, and the original study was approved by the local medical ethics committee. As it comprised a retrospective study, formal consent for the present analysis was not required. Subjects were referred to the UMCG and divided into three groups: healthy controls (HC) (n = 5), clinically diagnosed Parkinson's Disease patients (PD) (n = 8), and patients without a clear clinical diagnosis (n = 5). The latter group will be referred to as 'undiagnosed' (UD) throughout this paper. Patients in the PD group were diagnosed by a movement disorders specialist according to clinical consensus criteria[18].

Subjects fasted for a minimum of 4 h before the start of the scan and 2.5 mg/kg of carbidopa was administered orally. One hour after the carbidopa administration, subjects received an intravenous bolus injection of 200 MBq of [^{18}F]-FDOPA and were positioned in the high-resolution ECAT EXACT HR+ PET scanner (Siemens Healthcare, Erlangen, Germany) for a 2 h dynamic 3D PET acquisition started at time of injection. [^{18}F]-FDOPA was prepared

in the radiochemical laboratory of the University Medical Center Groningen according to a previously described synthesis protocol[19].

Image Processing

Individual PET data was corrected for scatter and randoms while a separate ellipse algorithm was used to correct for attenuation. Dynamic data was reconstructed using Direct Inverse Fourier transformation (DIFT)[20] and consisted of 21 frames (10 x 30 s, 3 x 300 s, 4 x 600 s and 4 x 900 s). All image post-processing was performed in PMOD (PMOD 3.3 Technologies Ltd, Zurich, Switzerland). First, motion correction was applied by using a weighted summation of the first 13 frames as reference for the rigid matching of the remaining, individual frames. Next, each dynamic PET dataset was spatially normalized to MNI space using an in house developed [^{18}F]-FDOPA specific brain template. Optimal transformation parameters were determined for the last 15 min time frame and subsequently applied to the dynamic dataset. A set of predefined volumes of interest (VOIs) derived from the Hammers atlas[21] was applied to the dynamic data and time activity curves (TACs) for the caudate nucleus, putamen and occipital cortex (reference region) were generated. Left and right sides of caudate and putamen VOIs were analyzed separately, since lateral differences in tracer kinetics can be observed within a single subject[22].

Image Analysis

First, PGA_{REF} was applied to all dynamic datasets, with the occipital cortex as reference tissue (PGA_{OCC}). Three different intervals were used to determine the PGA_{OCC} derived influx constant (K_i^{occ}). The starting point t* for the PGA_{OCC} analysis was fixed at 40 min p.i. to ensure that equilibrium was reached between plasma and non-displaceable, reversible tracer uptake, and the fitting was indeed restricted to the linear part of the PGA_{OCC} plot. Three different 15 min frames starting at 75, 90 and 105 min p.i. were used as end point for the PGA_{OCC} analysis. Values for K_i^{occ} obtained from PGA_{OCC} were referred to as $K_i^{occ}(40-\mathrm{X})$, with X representing the start of the 15 min frame at 75, 90 or 105 min p.i. These estimates were considered as ground truth for method comparison. For $K_i^{occ}(40-90)$ values, corresponding V_R estimates were also

reported for the caudate nucleus and putamen. To focus on the differences between the two striatal regions, data of the left and right hemisphere were pooled.

Second, corresponding K_{DTP}^{occ} values were determined using a dual time point approach (DTP_{OCC}) with the 10 min frame at 40 min p.i. as the first frame and three different 15 min frames starting at 75, 90 and 105 min p.i. as the second frame. Results were referred to as $K_{DTP}^{occ}(40-\mathrm{X})$ with X representing the start of the 15 min frame at 75, 90 or 105 min p.i. For each dataset, the $\overline{RPT}(t_1)$ of the occipital cortex at 40 min p.i was estimated by a population based average using the Leave One Out approach[23] (LOO), such that the individual $RPT(t_1)$ of each subject was excluded from the average value. To assess the validity of this approach, we evaluated the relative variability of $RPT(t)$ as function of time t p.i..

Finally, individual scans were also quantified using the SOR(X) of a single frame with X representing each of the three 15 min time frames starting at 75, 90 or 105 min p.i. respectively. In this way, SOR data were matched with the PGA_{OCC} and DTP_{OCC} analysis.

Statistical Analysis

DTP_{OCC} and SOR quantification were compared to PGA_{OCC} using linear regression and Pearson correlation analysis. A Bland-Altman plot was applied to analyze the agreement between PGA_{OCC} and DTP_{OCC}. Linear regression, Pearson correlation and Bland-Altman analysis were performed on all datasets, including HC, PD and UD data. Finally, a linear discriminant analysis (LDA) was conducted to investigate whether there were differences between methods when classifying subjects as HC or PD. The LDA was applied to PGA_{OCC} and DTP_{OCC} using the 40 to 90 min interval and to SOR using the 15 min frame starting at 90 min p.i. In this way, it was possible to compare results with literature data[12]. Left and right $K_i^{occ}(40-90)$ values and the corresponding V_R values of the two striatal regions were compared with a paired t-test.

To assess the effect of using a heterogeneous population based $\overline{RPT}(t_1)$ (n = 18) for the individual quantification of an incoming undiagnosed subject, we performed a two-step analysis. First, a non-parametric independent samples test (Mann-Whitney U) was used to

compare $RPT(t_1)$ values between the HC group and the group of PD patients. Next, another Mann-Whitney U test was performed to compare $\overline{RPT}(t_1)$ values between the group of pooled HC and PD subjects (n = 5 + 8) and the UD group (n = 5). Moreover, individual $\overline{RPT}(t_1)$ were compared to the corresponding LOO $\overline{RPT}(t_1)$ by means of a Bland-Altman analysis. For these analyses, t_1 = 40 min was used.

Results

Representative Patlak plots using the occipital cortex as a reference region are presented in Figure 1 for both HC and PD, with the Patlak plots of the PD patient displaying a modest lateralization for the putamen. PGA_{OCC} showed no significant differences between left and right $K_i^{occ}(40-90)$ values for both striatal regions (p = 0.13 for the caudate and p = 0.89 for the putamen). Corresponding V_R estimates were 0.99 ± 0.21 and 1.36 ± 0.11 (mean ± standard deviation) for caudate nucleus and putamen respectively. V_R values were significantly different ($p < 0.001$) between the two striatal regions.

Corresponding dual time point K_{DTP}^{occ} values showed excellent correlation with K_i^{occ} for all regions ($R^2 > 0.94$), as can be seen in Figure 2. Moreover, the slope of the linear regression analysis was close to one for all intervals and regions (Table 1). For all intervals, K_{DTP}^{occ} estimates for putamen demonstrated slightly better correlation with K_i^{occ} when compared to corresponding caudate estimates. The results of the Bland-Altman analysis were in agreement with the linear regression analysis, showing a region-dependent bias for the K_{DTP}^{occ} estimates. The range of the 95 % limits of agreement of the Bland-Altman analysis was relatively large, but the average bias remained under 7 % for all regions (Table 2).

Figure 3 represents the variability of $RPT(t)$ relative to the population average value as function of time t p.i.. The values for $RPT(40)$ were 50.1 ± 0.3, 46.3 ± 0.2 and 49.4 ± 0.1 for the HC, PD and UD group respectively (median ± interquartile range). There was a significant difference (Mann-Whitney U(13) = 3, z = -2.4, p = 0.011) between $RPT(40)$ values of the HC group and PD group. However, these differences remained small (7.9 % average difference). In addition, there were no significant differences between $RPT(40)$ values of the combined group of HC and PD subjects and those of the UD group, with a Mann-Whitney U(18) = 42, z = 0.93,

p = 0.38. The Bland-Altman analysis between individual $RPT(40)$ and corresponding LOO $\overline{RPT}(40)$ values demonstrated an excellent agreement between the estimates (0.16 % average bias). The 95 % limits of agreement indicated a percentage difference ranging from -12.4 % to 12.38 %. However, this range was primarily determined by one outlier with an individual $RPT(40)$ of 58.4 and a corresponding LOO $\overline{RPT}(40)$ of 48.4.

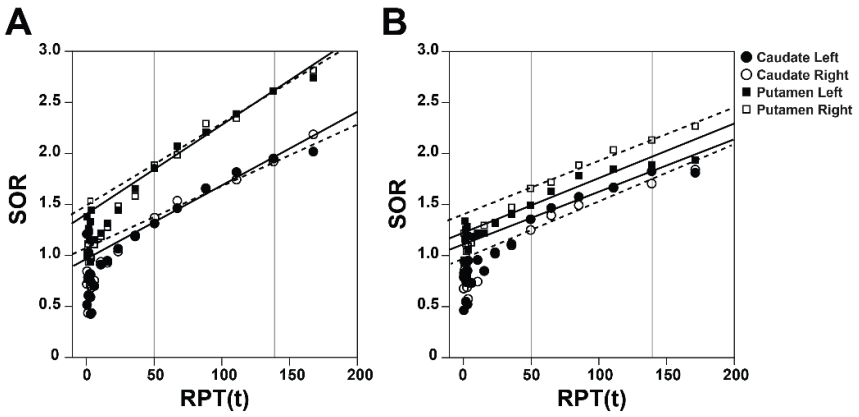

Figure 1. Representative PGA_{OCC} plots for a HC **(A)** and a PD **(B)** patient. Solid gray lines indicate the fitting interval (40 min - 90 min). For each region, the PGA_{OCC} fits are represented by solid black lines (left hemisphere) and dashed lines (right hemisphere).

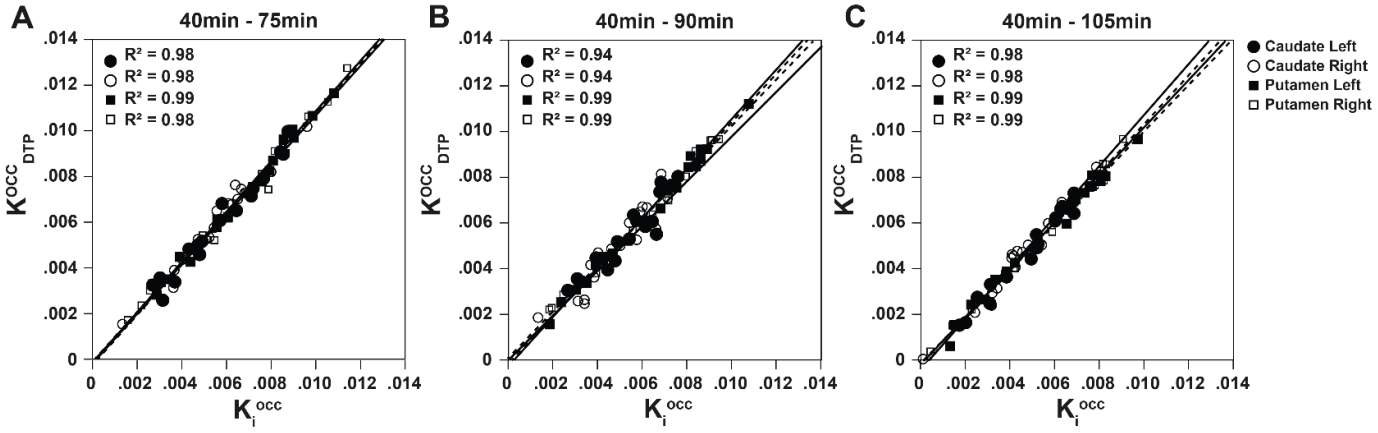

Figure 2. Comparison of the trapping rate estimated via DTP_{OCC} (K_{DTP}^{occ}) and via PGA_{OCC} (K_i^{occ}) for all striatal regions and for the three different intervals using linear regression analysis. R^2 values are similar for all regions and intervals ($R^2 > 0.94$), although a larger variability is seen for the 40 min - 90 min interval **(B)** compared to the 40 min - 75 min **(A)** and 40 min - 120 min **(C)** interval.

Overall, a good correlation was found between SOR and K_i^{occ} values (Figure 4). For the putamen, SOR showed an excellent correlation with K_i^{occ} estimates, especially for the 15 min frame starting at 105 min p.i. (R^2 values of 0.96 for the left putamen and 0.94 for the right putamen), while SOR values based on the two earlier frames presented a lower correlation with

K_i^{occ} estimates. For the caudate region, SOR generally displayed a lower correlation with the standard PGA_{OCC} approach compared to the putamen (Figure 4), although correlation improved with a later start time of the SOR frame. However, improvements were only modest, with R^2 values increasing from 0.36 to 0.56 for the left caudate and from 0.32 to 0.63 for the right caudate when the start time of the SOR frame was changed from 75 to 105 min p.i..

All three methods were able to classify HC and PD correctly (100 %). While the discriminant function (F test) did not suggest any significant differences in discriminative power between the three methods, the F ratio of the LDA proved to be region dependent (Table 3). The left putamen showed the highest discriminative power for all three methods ($K_i^{occ}(40 - 90)$: F = 69.8, $K_{DTP}^{occ}(40 - 90)$: F = 62.2 and SOR(90): F = 80.6) while the left caudate nucleus displayed the lowest values. For all methods, an overlap of the quantitative endpoints between the HC and PD group can be observed for the caudate nucleus, but not for the putamen (Figure 5).

Discussion

Although dynamic PET imaging may contribute to a more comprehensive understanding of underlying physiological processes, simple and short acquisition protocols are more suited for clinical routine[24]. Consequently, static PET scans at late time points after tracer injection are favored over long dynamic scanning protocols. However, static scans do not provide dynamic information, which might be of importance for detecting subtle changes during treatment or for monitoring disease progression. A dual time point approach aims at bringing together the advantages of static PET imaging with the ability to estimate the appropriate quantitative dynamic parameters. This study extended the mathematical derivation of a dual time point approach previously developed for [^{18}F]-FDG[9] to a reference tissue model DTP_{REF} for quantifying irreversible tracer binding. Its implementation is simple and utilizes only 1) two static scans at different time points p.i. and 2) a population based average of the normalized area under the curve of the tracer uptake in the reference region for the time interval between the start of the scan and the first time point p.i. Based on the information of two static scans, DTP_{REF} has as its main outcome the influx or trapping rate constant K_{DTP}^{REF} of the tracer,

which is a direct approximation of K_i^{REF}. As the DTP_{REF} approximation is applicable for PET tracers such as [^{18}F]-FDOPA, this approach was validated for [^{18}F]-FDOPA brain PET imaging using a heterogeneous group of healthy controls, probable PD and undiagnosed patients.

Table 1. Results of the linear regression analysis between K_{DTP}^{occ} and K_i^{occ} for all regions and intervals. The linear fits are close to the line of identity of all regions and intervals, while R^2 values are close to one.

		Interval					
		40 min - 75 min		40 min - 90 min		40 min - 105 min	
		Slope	R^2	Slope	R^2	Slope	R^2
Caudate	left	1.08	0.98	0.98	0.94	1.07	0.98
	right	1.11	0.98	1.08	0.94	1.11	0.98
Putamen	left	1.08	0.99	1.06	0.99	1.02	0.99
	right	1.09	0.99	1.01	0.99	1.04	0.99

In the case of [^{18}F]-FDOPA, the corresponding trapping rate relates to the striatal dopamine storage capacity. The comparison between the trapping rates estimated from both the DTP_{OCC} method and the standard PGA_{OCC} using occipital cortex as reference region showed good correspondence between the methods (Figure 2 and Table 1). The correlation and linear regression analysis demonstrated an overall strong correlation between the two methods as well as a slope close to one, therefore validating the DTP_{REF} approximation. Nevertheless, the correlation was consistently higher for the putamen, and the estimates for the caudate region seemed to show greater variability.

Table 2. Results of the Bland-Altman analysis comparing K_{DTP}^{occ} and K_i^{occ} values for each region and interval. All regions demonstrate a small bias (< 7%), which increases as the interval time decreases. The 95 % limits of agreement (L.A.) show a wide range, independent of the interval.

		Interval					
		40 min - 75 min		40 min - 90 min		40 min - 105 min	
		% Bias	95 % L.A.	% Bias	95 % L.A.	% Bias	95 % L.A.
Caudate	Left	3.9 ± 8.9	-13.5 to 21.4	3.3 ± 9.8	-15.8 to 22.5	-1.3 ± 8.6	-18.3 to 15.6
	Right	5.6 ± 7.5	-9.1 to 20.2	1.9 ± 16.5	-30.5 to 34.3	-0.9 ± 12.8	-26.1 to 24.2
Putamen	Left	6.1 ± 5.7	-5.0 to 17.2	2.3 ± 5.3	-8.1 to 12.6	-2.6 ± 15.2	-32.3 to 27.1
	Right	4.4 ± 6.2	-7.7 to 16.6	4.0 ± 6.9	-9.5 to 17.6	0.9 ± 5.0	-9.4 to 10.2

Such regional differences in correlations between DTP_{OCC} and standard PGA_{OCC} are in agreement with other studies comparing quantification methods for [^{18}F]-FDOPA brain PET[12,25]. Specifically for the DTP_{OCC} approach, these regional differences could be explained by the smaller VOI size and the limited count statistics of the caudate nucleus compared to the putamen. Whereas a standard PGA_{OCC} uses multiple time frames for the quantification, DTP_{OCC} only takes into account two time frames, making it more sensitive to noise and small misalignments.

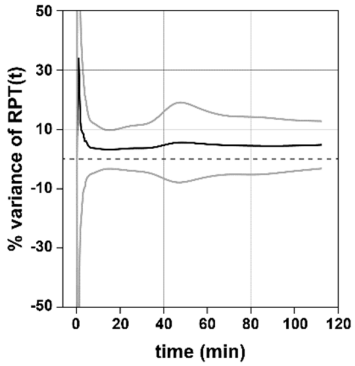

Figure 3. This graph shows the variability of $RPT(t)$ relative to the population average (n = 18) $\overline{RPT}(t)$ as function of time t p.i.. The solid black line represents the average variance between individual and population $RPT(t)$ relative to $\overline{RPT}(t)$, defined as (($RPT(t)$ - $\overline{RPT}(t)$) / $\overline{RPT}(t)$) x 100 %. The solid gray lines represent the upper and lower limit, defined as mean ± 1.96 x SD.

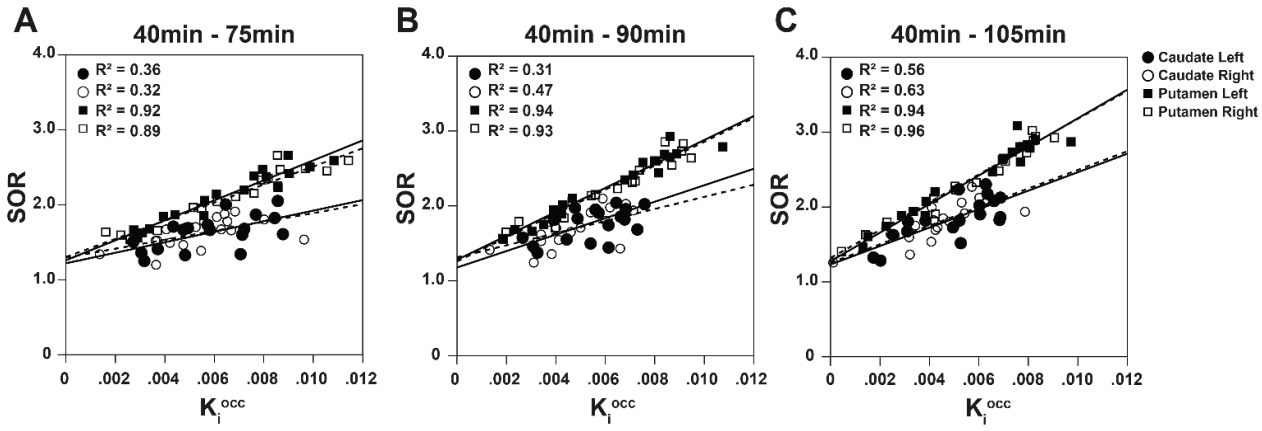

Figure 4. Comparison of methods by means of linear regression analysis of SOR and K_i^{occ} for all regions and three different intervals. R^2 values are consistently higher for putamen than for the corresponding caudate regions. For the later intervals, there is an increase in R^2 values for all regions, with the highest value corresponding to the 40 min - 105 min interval **(C)** in comparison to 40 min - 75 min **(A)** and 40 min - 90 min **(B)** interval. For the caudate region, however, R^2 values are not as high as for the putamen, even for the latest interval.

When evaluating quantification methods for [^{18}F]-FDOPA brain PET, previous studies have pooled left and right regions, in contrast to the methodological approach of this study. While our results showed no statistical significance between left and right K_i^{occ} values for both regions, the left side did demonstrate higher F-ratios for both the caudate nucleus and putamen. Other studies have shown that lateralization is indeed a well-known characteristic of Parkinson's Disease and patients often show a symptom dominant side[26]. Therefore, pooling of left and right striatal regions could generate fictitiously larger trapping rates or improve model fits, a strategy which has been applied previously[12,27]. However, it is advisable to avoid merging hemispheres and potentially different kinetics when evaluating the performance of different quantitative methods.

Table 3. Linear discriminant analysis (F ratio) for all three quantitation methods. The F ratio describes the separation between the HC and PD groups for each of the striatal regions analyzed in this study.

Method	F ratio			
	Caudate (right)	Caudate (left)	Putamen (right)	Putamen (left)
K_i^{occ} (40-90)	8.3	5.9	48.5	69.8
K_{DTP}^{occ} (40-90)	9.0	9.16	61.9	63.9
SOR (90)	11.8	10.2	52.9	80.6

An important parameter affecting the performance of the presented methods is the interval of the time frames chosen for the quantification. Previous studies suggest [^{18}F]-FDOPA can only be considered as a truly irreversible tracer until 90 min after injection (or earlier in disease states)[14,28,29]. We applied PGA_{OCC} and DTP_{OCC} to intervals with the final frame starting earlier and later than 90 min p.i in order to evaluate the performance of the quantification methods for different tracer kinetics. The results of the linear regression (Table 1) and the Bland-Altman analysis (Table 2) suggested that both methods are providing comparable estimates despite possible deviations from true irreversible tracer kinetics. However, the Bland-Altman results revealed a wide range for the 95 % limits of agreement, although the average bias remained under 7 % for all regions and time intervals. This wide range for the limits of agreement was caused by two very small K_i^{occ} values in the PD group which proved to have slightly different K_{DTP}^{occ} values.

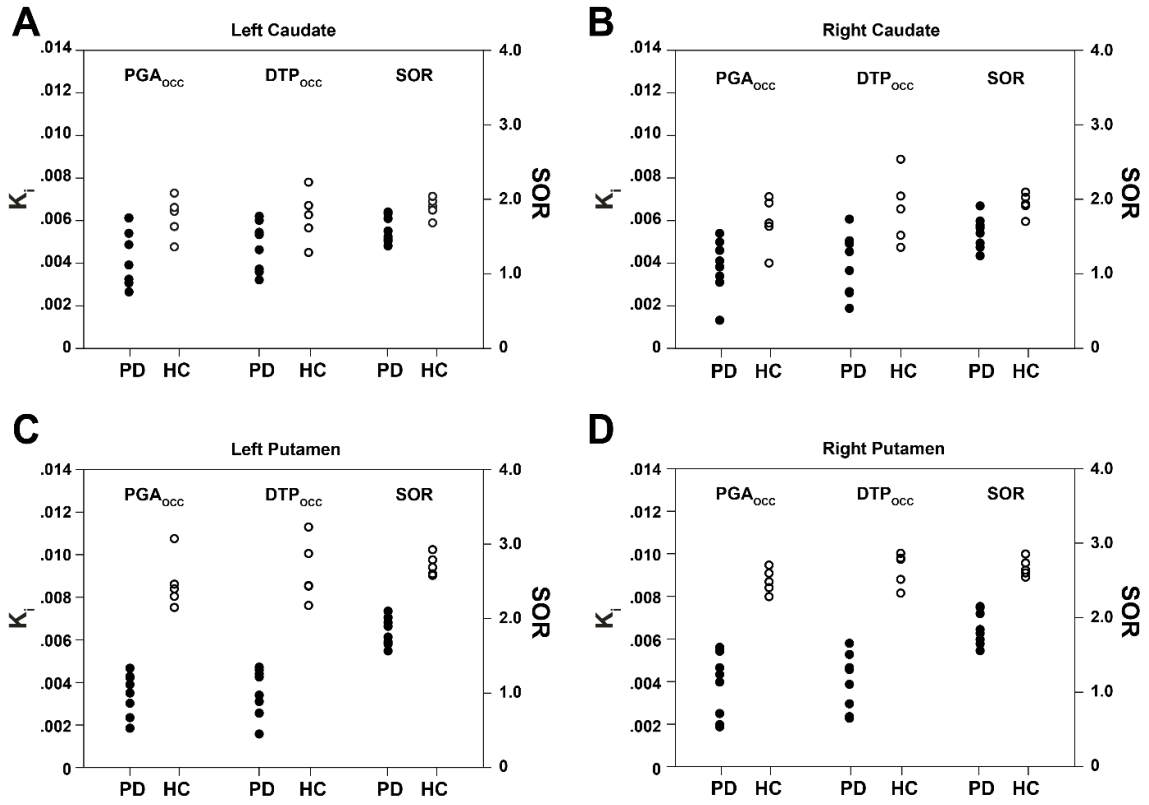

Figure 5. Linear discriminant analysis per region demonstrating the classification of the different groups based on each method. All three methods are able to classify HC and PD with a 100 % accuracy based on the quantification results for the putamen ((**C**) and (**D**)) while an overlap between groups is observed for the caudate region ((**A**) and (**B**)).

An important characteristic of the DTP_{OCC} method is the use of a population average $\overline{RPT}(40)$ for individual quantification. Results from a Mann-Whitney U test confirmed that there were no significant differences between $\overline{RPT}(40)$ values of the combined groups of HC and PD (HC+PD) and the UD group ($p = 0.38$). Moreover, although the largest difference in $RPT(40)$ values, observed between the HC and PD groups, was statistically significant ($p = 0.01$), this difference was still small (7.9 %). In a practical scenario, this indicates that for $t_1 = 40$ min, a population $\overline{RPT}(40)$ could be used for new patients irrespective of the disease state of these patients. Even in cases of a larger discrepancy between individual $RPT(40)$ and LOO $\overline{RPT}(40)$, the K_{DTP}^{occ} estimates were not greatly affected. Finally, the average difference between K_{DTP}^{occ} values determined by an individual $RPT(40)$ and by a LOO $\overline{RPT}(40)$ was of only 8% for all regions. In line with these results, previous studies[5,30] found population average input

functions to be applicable for individual quantification via PGA. Similarly, our results support the concept of a subject independent, normalized time activity curve of the occipital cortex. This was demonstrated graphically in Figure 3, showing the limited relative variability of $RPT(t)$ for all time points t p.i.. Based on these findings, it is reasonable to approximate an individual DTP_{OCC} quantification with a population based average $\overline{RPT}(40)$. According to the limited relative variability of the $RPT(t)$ (Figure 3), an average value could also be considered for the second time point at 90 min p.i. (Equation (6)). Although such a setting could further simplify the DTP_{REF} method, it should be considered for each tracer separately. For [^{18}F]-FDOPA, a large reference region with favorable statistics is available in the form of the occipital cortex, and the measured data can directly provide a reliable, individual $RPT(90)$ estimate for the DTP_{OCC} approach, eliminating the need for a population average value beyond the time point t_1 and avoiding unnecessary *a priori* assumptions. However, other irreversible tracers might present a smaller reference region or a region with limited statistics, such that a full population based approach could be less affected by noise, and therefore prove favorable.

To contextualize the DTP_{OCC} approximation with a clinically used simplified approach, the performance of SOR was also assessed. Results showed that the slope of the linear regression analysis between SOR and K_i^{occ} was lower for the caudate nucleus compared to the putamen. This can be explained by the linear relationship between SOR and K_i^{occ} (Equation (1)), which is determined by V_R and $RPT(t)$ with t the frame time for SOR quantification. Since $RPT(t)$ is identical for both striatal regions, the different linear relationship between SOR and K_i^{occ} can only be caused by the significantly lower V_R values of the caudate nucleus compared to the putamen. Furthermore, correlations between SOR and K_i^{occ} proved to be different for the caudate nucleus and putamen with SOR values of the caudate region displaying a weaker correlation with K_i^{occ} values compared to the putamen. Since $RPT(t)$ values exhibit only very modest inter-subject variability (Figure 3), correlations between SOR and PGA_{OCC} are mainly affected by the high inter-subject variability of the V_R estimates for both striatal regions. Because of the lower inter-subject variability of V_R values for the putamen, a stronger correlation is observed between SOR and PGA_{OCC} for that region. This inter-subject variability of V_R might be caused by different physiological conditions between subjects, but also by small deviations

from the PGA model assumptions, the limited count statistics of the different time frames used for the PGA model, and potential motion between the time frames. In that sense, PGA_{OCC} and DTP_{OCC} methods are affected in a similar way, which explains the higher correlation between both compared to correlation between SOR and PGA_{OCC} (Figure 2 and 4). On the other hand, SOR uses only a single frame, thus avoiding computing differences between time frames, which can introduce corresponding statistical errors. Moreover, the SOR approach is less sensitive to patient motion and small misalignments. This could explain the distinctly lower intra-group variability of SOR in the discriminant analysis compared to PGA_{OCC} or DTP_{OCC}.

Nonetheless, all methods were able to classify HC and PD with 100 % accuracy. However, SOR seemed to better discriminate the two groups, showing a generally higher F ratio for all regions compared to PGA_{OCC} and DTP_{OCC} (Table 3). The results of this study regarding the comparison between SOR and K_i^{occ} can be considered somewhat contrasting to what was previously reported[12], both in terms of correlation and discriminative power. Such a discrepancy might be explained by methodological differences (such as VOI definition and left-right VOI separation) and population size. It should also be noted that the population in this study is small, which could limit an accurate assessment of the discriminative power of the tested methods. However, within the limits of the present study, SOR can still be considered as the best clinical parameter for group discrimination. It is important to notice that all three methods (DTP_{OCC}, PGA_{OCC} and SOR) can be biased by [^{18}F]-FDOPA radiometabolites entering the brain. More specifically, all methods rely on the whole TAC of the reference region as input function, without any prior correction for radiometabolites. Therefore, the possible limitation of a metabolite induced bias is inherent to all three methods, with corresponding results being affected in a similar way.

In general, unlike PGA_{REF}, the DTP_{REF} method relies on information from only two time frames instead of the whole TAC. Consequently, the approximation is more sensitive to noise than PGA_{REF}. Hence, frame durations and reconstruction algorithms need to be chosen appropriately in order to minimize bias. Moreover, the patient is repositioned in the PET system for the acquisition of the second time point, which turns image registration between the two time points mandatory. In current clinical practice, [^{18}F]-FDOPA brain PET imaging is

performed on PET/CT systems such that the low-dose CT scan of each PET/CT scanning session can easily be used to coregister the PET data of the two time points, independent of potential differences in the PET emission patterns between the two scans.

The DTP_{OCC} protocol provides a reduction in scanning time ranging from 90 min to 120 min to approximately 30 min without compromising dynamic information. Based on our results, we suggest the acquisition of two static 10 min frames at 40 min and 90 min p.i. for DTP_{OCC} quantification of [^{18}F]-FDOPA brain PET imaging. This would translate into approximately 30 min of free camera time between the two consecutive time points (taking into account an extra 5 min for patient positioning in between scans). This interval could be used for an extra whole body PET scan or the scanning of one time point of another DTP_{OCC} [^{18}F]-FDOPA brain scanning protocol, which would significantly increase patient throughput. With current state of the art PET systems[31], even shorter static acquisitions could be considered due to the higher PET system sensitivity, further reducing the scanning time. Our results suggest that DTP_{OCC} imaging of [^{18}F]-FDOPA uptake in the brain is an enhanced combination of static imaging and dynamic information, representing a valuable, simplified quantification of brain dopaminergic function in both PD patients and healthy controls. The DTP_{OCC} method is also able to avoid long acquisition protocols and therefore increase patient comfort. This is especially important in the context of an older population, as is the general case for PD patients. Moreover, shorter scans are preferable for PD patients since they reduce the chance of head movement during the image acquisition, therefore increasing image quality and quantitative accuracy.

The reference tissue dual time point method DTP_{OCC} was able to reliably estimate the trapping rate K_i^{occ} in [^{18}F]-FDOPA brain PET imaging while achieving the same discriminative power between PD patients and healthy controls as PGA_{OCC}. The use of DTP_{OCC} allowed a simplification of [^{18}F]-FDOPA imaging protocols by shortening the overall acquisition time while maintaining the relevant dynamic information. In general, the proposed DTP_{REF} method provides a valid approximation of the standard PGA_{REF} and therefore can be considered for estimating the trapping or metabolization rate of other irreversible PET tracers, provided that

a reference tissue is available. As such, the DTP_{REF} approach can become a valuable tool to quantify irreversible tracer binding using a reference tissue.

Acknowledgements

The authors would like to personally acknowledge David Vállez García and Luis Eduardo Juárez Orozco for their support and contribution to the statistical analysis of the results.

REFERENCES

1. Patlak, C. S., Blasberg, R. G. & Fenstermacher, J. D. Graphical evaluation of blood-to-brain transfer constants from multiple-time uptake data. *J. Cereb. Blood Flow Metab.* **3,** 1–7 (1983).
2. Patlak, C. S. & Blasberg, R. G. Graphical evaluation of blood-to-brain transfer constants from multiple-time uptake data. Generalizations. *J. Cereb. Blood Flow Metab.* **5,** 584–90 (1985).
3. Boellaard, R. Standards for PET image acquisition and quantitative data analysis. *J. Nucl. Med.* **50 Suppl 1,** 11S–20S (2009).
4. Ikoma, Y. *et al.* Evaluation of semi-quantitative method for quantification of dopamine transporter in human PET study with 18F-FE-PE2I. *Ann. Nucl. Med.* (2015). doi:10.1007/s12149-015-0993-3
5. van den Hoff, J. *et al.* The PET-derived tumor-to-blood standard uptake ratio (SUR) is superior to tumor SUV as a surrogate parameter of the metabolic rate of FDG. *EJNMMI Res.* **3,** 77 (2013).
6. Keyes, J. W. SUV: standard uptake or silly useless value? *J. Nucl. Med.* **36,** 1836–9 (1995).
7. Thie, J. A. Understanding the standardized uptake value, its methods, and implications for usage. *J. Nucl. Med.* **45,** 1431–1434 (2004).
8. Basu, S. & Alavi, A. Partial volume correction of standardized uptake values and the dual time point in FDG-PET imaging: Should these be routinely employed in assessing patients with cancer? *Eur. J. Nucl. Med. Mol. Imaging* **34,** 1527–1529 (2007).
9. den Hoff, J. van *et al.* Dual time point based quantification of metabolic uptake rates in 18F-FDG PET. *EJNMMI Res.* **3,** 16 (2013).
10. Firnau, G. *et al.* [18F]Fluoro-l-dopa for the in vivo study of intracerebral dopamine. *Int. J. Radiat. Appl. Instrumentation. Part A. Appl. Radiat. Isot.* **37,** 669–675 (1986).
11. Loane, C. & Politis, M. Positron emission tomography neuroimaging in Parkinson's disease. *Am. J. Transl. Res.* **3,** 323–341 (2011).
12. Dhawan, V. *et al.* Comparative analysis of striatal FDOPA uptake in Parkinson's disease: ratio method versus graphical approach. *J. Nucl. Med.* **43,** 1324–30 (2002).
13. Jaimini, A. *et al.* Utility of intrastriatal ratios of FDOPA to differentiate idiopathic Parkinson's disease from atypical parkinsonian disorders. *Nucl. Med. Commun.* **34,** 426–31 (2013).
14. Jokinen, P. *et al.* Simple Ratio Analysis of 18F-Fluorodopa Uptake in Striatal Subregions Separates Patients with Early Parkinson Disease from Healthy Controls. *J. Nucl. Med.* **50,** 893–899 (2009).
15. Sossi, V., Doudet, D. J. & Holden, J. E. A reversible tracer analysis approach to the study of effective dopamine turnover. *J. Cereb. Blood Flow Metab.* **21,** 469–76 (2001).
16. Holden, J. E. *et al.* Graphical analysis of 6-fluoro-L-dopa trapping: effect of inhibition of catechol-O-methyltransferase. *J. Nucl. Med.* **38,** 1568–1574 (1997).
17. Sossi, V. *et al.* Increase in dopamine turnover occurs early in Parkinson's disease: evidence from a new modeling approach to PET 18 F-fluorodopa data. *J. Cereb. Blood Flow Metab.* **22,** 232–9 (2002).
18. Hughes, A. J., Daniel, S. E., Kilford, L. & Lees, A. J. Accuracy of clinical diagnosis of idiopathic Parkinson â€™ s disease : a clinico-pathological study of 100 cases. 181–184 (1992). doi:10.1136/jnnp.55.3.181

19. de Vries, E. F. ., Luurtsema, G., Brüssermann, M., Elsinga, P. H. & Vaalburg, W. Fully automated synthesis module for the high yield one-pot preparation of 6-[]fluoro-l-DOPA. *Appl. Radiat. Isot.* **51,** 389–394 (1999).
20. Stearns, C. W., Chesler, D. A. & Brownell, G. L. Three Dimensional Image Reconstruction in the Fourier Domain. *IEEE Trans. Nucl. Sci.* **34,** 374–378 (1987).
21. Hammers, A. *et al.* Three-dimensional maximum probability atlas of the human brain, with particular reference to the temporal lobe. *Hum. Brain Mapp.* **19,** 224–247 (2003).
22. Leenders, K. L. *et al.* The nigrostriatal dopaminergic system assessed in vivo by positron emission tomography in healthy volunteer subjects and patients with Parkinson's disease. *Arch. Neurol.* **47,** 1290–8 (1990).
23. Arlot, S. & Celisse, A. A survey of cross-validation procedures for model selection. *Stat. Surv.* **4,** 40–79 (2010).
24. Carson, R. E. Precision and accuracy considerations of physiological quantitation in PET. *J. Cereb. Blood Flow Metab.* **11,** A45-50 (1991).
25. Hoshi, H. *et al.* 6-[18F]fluoro-L-dopa metabolism in living human brain: a comparison of six analytical methods. *J. Cereb. Blood Flow Metab.* **13,** 57–69 (1993).
26. Cheesman, A. L. *et al.* Lateralisation of striatal function: evidence from 18F-dopa PET in Parkinson's disease. *J. Neurol. Neurosurg. Psychiatry* **76,** 1204–10 (2005).
27. Pavese, N. *et al.* [18F]FDOPA uptake in the raphe nuclei complex reflects serotonin transporter availability. A combined [18F]FDOPA and [11C]DASB PET study in Parkinson's disease. *Neuroimage* **59,** 1080–1084 (2012).
28. Sossi, V. *et al.* Changes of dopamine turnover in the progression of Parkinson's disease as measured by positron emission tomography: their relation to disease-compensatory mechanisms. *J. Cereb. Blood Flow Metab.* **24,** 869–76 (2004).
29. Oehme, L. *et al.* Comparison of dopamine turnover, dopamine influx constant and activity ratio of striatum and occipital brain with 18F-dopa brain PET in normal controls and patients with Parkinson's disease. *Eur. J. Nucl. Med. Mol. Imaging* **38,** 1550–1559 (2011).
30. Hofheinz, F. *et al.* Comparative evaluation of SUV, tumor-to-blood standard uptake ratio (SUR), and dual time point measurements for assessment of the metabolic uptake rate in FDG PET. *EJNMMI Res.* **6,** 53 (2016).
31. Jakoby, B. W. *et al.* Physical and clinical performance of the mCT time-of-flight PET/CT scanner. *Phys. Med. Biol.* **56,** 2375–2389 (2011).